Published by :
https://www.ijert.org/
An International Peer-Reviewed Journal

International Journal of Engineering Research & Technology (IJERT)
ISSN: 2278-0181
Vol. 15 Issue 05 , May - 2026

Numerical Investigation of 2D DJ Phase Perovskite Solar Cells Using SCAPS-1D

Shrivilas Mishra, Rishabh Yadav, Harsh Bansal, Ujjwal Singh, Dr. Pooja Lohia
Department of Electronics and Communication Engineering
Madan Mohan Malaviya University of Technology (MMMUT)
Gorakhpur, Uttar Pradesh, 273010, India

Abstract - DJ (Dion-Jacobson) two-dimensional (2D) bipolar materials can provide the improved stability of a three-dimensional (3D) perovskite, while demonstrating comparable efficiencies to 3D perovskites. Furthermore, the purpose of this study was to simulate how the 2D DJ material in a thin film photovoltaic device built on an ITO/SnO_2/$(BDA)(MA)_3Pb_4I_{13}$ (n=4)/Spiro-OMeTAD/Au structure would perform when using SCAPS-1D simulation software. Using ideal conditions (V_{OC}=1.2493 V, J_{SC}=23.59 mA/cm² and FF=83.36%), the DJ perovskite $(BDA)(MA)_3Pb_4I_{13}$ (n=4) has an EG value of 1.62 eV and has a calculated PCE of 24.57%. When accounting for realistic optical filtering, the PCE drops to 22.09% (Voc = 1.2445 V, J_{SC} = 21.26 mA/cm², FF=83.49%), a difference of 2.5% absolute loss that is also consistent with experimental results. Additionally, performing quantum efficiency measurements reveals >95% EQE in the 400-650nm spectral region under ideal conditions, and ~90% when applying realistic optical attenuation. Therefore, the use of a SnO_2/DJ-2D perovskite/Spiro-OMeTAD architecture can create, with potential efficiencies of ~25%, a commercially viable photovoltaic device by optimizing and addressing optical losses.

Keywords - Perovskite-based technologies, photovoltaic solar module technology, Optical loss due to Dion-Jacobson phase, Performance optimization of PSCs.

I. INTRODUCTION

Photovoltaic technology presents one viable option for addressing the increasing global energy crisis; however, continued reliance on fossil fuels is a significant contributor to global warming and its impact on human health is becoming more apparent with each passing day. The theoretical maximum efficiency of traditional crystalline-silicon-based solar cells has been estimated to be about ~29% when illuminated by AM1.5G (1 sun). Therefore, in order to meet the growing demand for renewable energy sources and achieve next generation photovoltaic technologies that will reach efficiencies far beyond those currently achieved by crystalline silicon photovoltaic devices [1].

Since 2009 organic-inorganic halide perovskite materials described by the ABC3 formula where A = Monovalent cation, B = Divalent Metal Cation (Mostly Lead), and C = Halide anion have been an important research area in solar cell solutions. These materials have excellent optoelectronic characteristics with wide bandgap tunability (1.2 to 3.5 eV), high absorption coefficient (>104 cm-1s), long diffusion length of charge carriers (>1 µm) [2]. Three-dimension (3D) perovskite solar cells have demonstrated performance at over 26.1% PCE; however, due to poor atmospheric stability, high ionic migratory energy and the toxic nature of lead, these solar cells' potential is currently limited. Conversely, the addition of large cation based on organic compounds in between octahedral units of the ammonium lead halide provides greater chemical and thermal stability, reduced ionic migration, and enhanced resistance against environmental conditions compared to conventional 2D perovskite solar cells that use between layer ammonium based spacer cation compounds as opposed to the more conventional Ruthenium based spacer cation compounds, respectively. The Dion-Jacobson (DJ) structure using monoammonium based spacer cations shows comparable interlayer electronic coupling performance index than that observed from conventional Ruddlesden-Popper structured perovskite solar cells utilizing Ruddlesden-Popperspacer cation compounds. In general DJ structure devices have demonstrated significant operational stability with >92% performance improved from continuous operation for approximately 6000 hours at 45°C. The specific composition of the DJ (Dion-Jacobson) $(BDA)(MA)_3Pb_4I_{13}$ (n=4) is ideal for a trade-off between optoelectronic properties and long-term stability; the bandgap of this specific DJ composition is measured to be 1.62 eV. This bandgap value indicates that this specific DJ composition would be well-suited for solar spectrum photonic energy generation [3], [4]. The electron transport layer (ETL) for this specific ITO/SnO_2/$(BDA)(MA)_3Pb_4I_{13}$/Spiro-OMeTAD/Au heterojunction design is tin oxide (SnO2), which has both a high electron mobility and an optimal band alignment with the underlying perovskite absorber layer. The hole transport layer (HTL) of this device is Spiro-OMeTAD, providing a high-hole mobility when appropriately doped and is well established to have p-type doping chemistry [5], [6].

This study utilises an n-type SnO_2 (ETL) in conjunction with a 2D Dion-Jacobson (DJ) perovskite $(BDA)(MA)_3Pb_4I_{13}$ (absorber) and a p-type Spiro-OMeTAD (HTL) to construct a complete photovoltaic device architecture. The SCAPS-1D simulation software was used to optimise the device layers of the ITO/SnO_2/$(BDA)(MA)_3Pb_4I_{13}$/Spiro-OMeTAD/Au heterojunction design through sequentially modifying the design until an optimum device configuration was achieved. In particular, the effects of absorber layer thickness (ranging from 0.4 to 1.6 µm) and defect density minimisation (ranging from 1.0×10^{10} to 1.0×10^{20} cm^{-3}) on the final device performance were investigated. In order to thoroughly investigate the device architecture, optical filtering and band alignment were

International Journal of Engineering Research & Technology (IJERT)
ISSN: 2278-0181
Vol. 15 Issue 05 , May - 2026

investigated. The temperature of the device was maintained at 300 K to establish a baseline for device performance evaluation.

With the use of systematic simulation refinement, the material properties and device configurations were optimised to achieve the best performing 2D Dion–Jacobson perovskite solar cell design. Under perfect optical conditions, the device achieved a peak power conversion efficiency of 24.57 %. However, when real-world optical filtering effects were included in the simulation, this efficiency was reduced to approximately 22.09 % due to a loss of approximately 2.5 % absolute due to primarily parasitic absorption in front contact layers.

II. DEVICE STRUCTURE AND SIMULATION METHOD

The University of Gent in Belgium created a program called SCAPS-1D (Solar Cell Capacitance Simulation - 1 Dimension). The program uses mathematical models to estimate how well solar cells will perform using a combination of the Poisson equation and the Drift Diffusion Carrier Transport Equations to generate J-V curves, efficiency values, and charge distributions, and the inter-electrostatic field in the solar cell (by generating internal electric field distributions and calculating the total charge, then dividing that by the total area of the cell. This simulation can also provide insight into how different wavelengths of light will interact with solar cells. This is accomplished by using the Poisson equation along with carrier continuity equations for electrons and holes to calculate either a V-I response directly (using the equations for Poisson) or via calculating V-I response in the electric field from the two equations (1–3) [7], [8].
The change in electric potential across the device can be described by the following relation:

$$\frac{d}{dx}\left(-\varepsilon(x)\frac{d\emptyset}{dx}\right) = [p(x) - n(x) + N_D(x) - N_A(x) + p(x) - n(x)] \quad (1)$$

In this equation, the parameters p, N_A, and N_D refer to hole concentration and the acceptor and donor densities of dopants, respectively. The variables n(x) and p(x) indicate the variation in hole and electron concentrations as a function of distance along the device, and the symbol ε represents the material's relative permittivity. Through the continuity framework, all mobile charge carriers are conserved and follow a continuous path throughout their transport, generation and recombination processes throughout the device.

The rate of change of the number density of the electrons at any point in space evolves according to the following:

$$\frac{\partial n(x,t)}{\partial t} = \frac{1}{q}\frac{\partial J_n}{\partial x} + G_n(x,t) - R_n(x,t) \quad (2)$$

The hole concentration momentum can also be derived as follows:

$$\frac{\partial p(x,t)}{\partial t} = \frac{1}{q}\frac{\partial J_p}{\partial x} + G_p(x,t) - R_p(x,t) \quad (3)$$

where G_n is the electron generation rate and R_n is the electron recombination rate, whereas G_p is the photogeneration of holes and R_p is the recombination of holes.

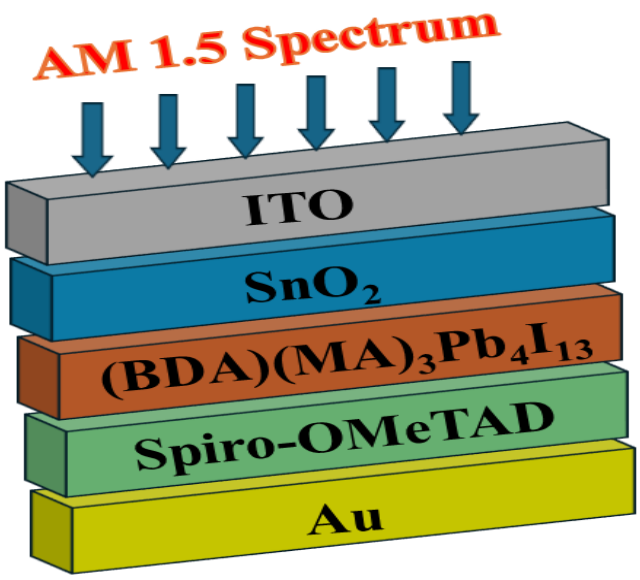

(a)

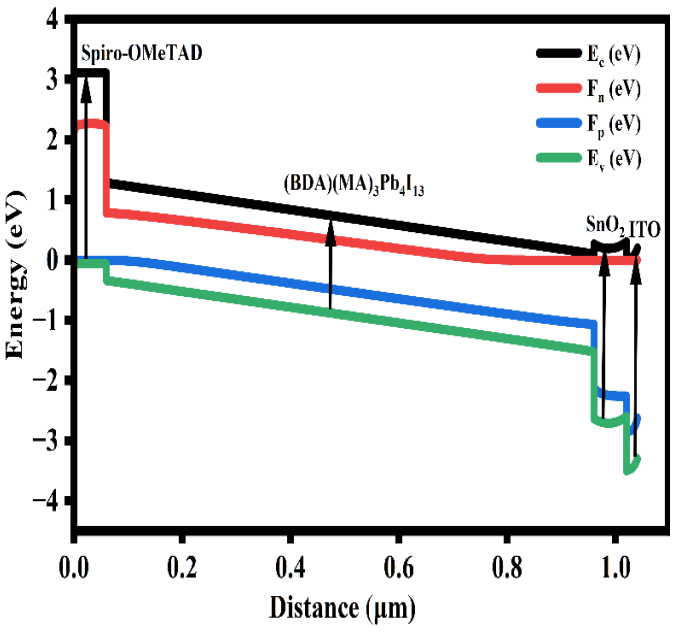

(b)

International Journal of Engineering Research & Technology (IJERT)
ISSN: 2278-0181
Vol. 15 Issue 05 , May - 2026

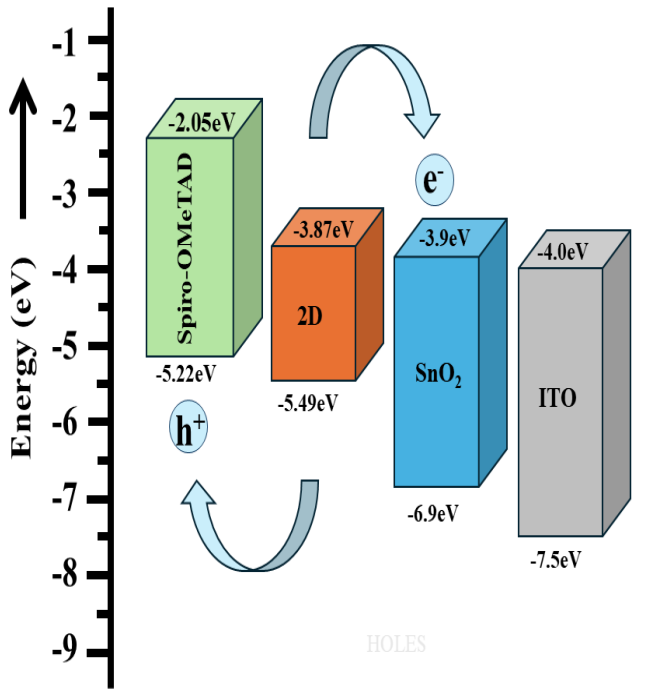

(c)

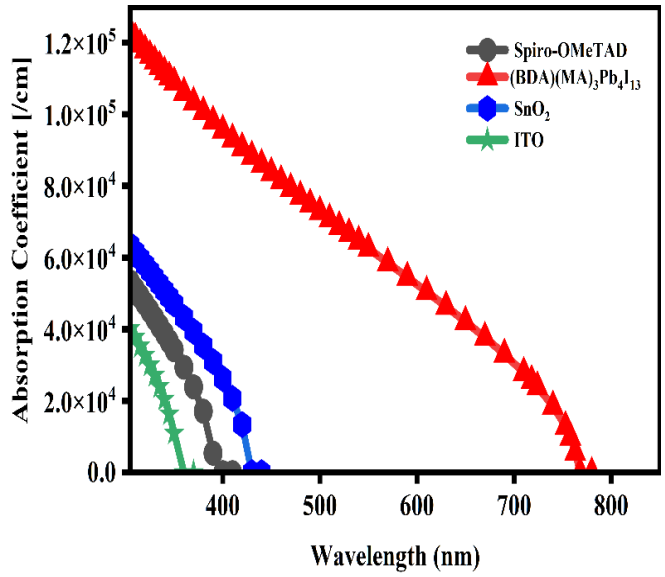

(d)

Fig. 1. (a): A proposed DJ 2D PSC architecture; (b) Energy band structure (c) Band alignment diagram showing electronic energy levels across device thickness; (d) Absorption spectra of materials used in solar cell.

Figure 1. provides an overview of the electronic properties and architecture of the device being evaluated. **Figure 1. (a)** shows the layered construction of the device where the first layer is a transparent indium tin oxide anode followed by a tin oxide electron transport layer. It is then followed by a two-dimensional Dion-Jacobson perovskite $(BDA)(MA)_3Pb_4I_{13}$ absorber layer, Spiro-OMeTAD hole transport layer, and an Au back contact. Each of these layers is configured to be subjected to the standard AM1.5G solar incident spectrum. The parameters for each of the materials used to create the layers and the physical thickness of the layers are detailed in **Table 1**. Using the data from **Table 1** will allow for an easy understanding of the components of the device that are necessary to perform SCAPS-1D numerical simulations including the E_g, χ, ε_r, N_C, N_V of the various materials that comprise the device.

Figure 1(b) illustrates the conduction band minimum (E_C in black), the electron quasi-Fermi level (E_{fn} in red) and the hole quasi-Fermi level (E_{fp} in blue), and the valence band maximum (E_V in green) plotted as a function of device depth, ranging from 0-1.0 µm. The heterojunction formed between the two materials (perovskite and the charge transport layers) is of Type II in nature where the two quasi-Fermi levels for electrons and holes become separated. This separation of the quasi-Fermi levels indicates that the two interfaces effectively separate the charge carriers. Therefore, with this type of heterojunction the electrons are induced to drift toward the SnO_2 ETL on one side of the perovskite, while the holes drift toward the Spiro-OMeTAD layer at the opposite interface; this promotes reduced radiative and non-radiative recombination. **Figure 1(c)** shows the band structures of the various materials and the relative positions of the CBM and the VBM, along with the corresponding values for their bandgaps that were derived from the parameters listed in **Table 1**. The arrows in the figure indicate how the carriers are expected to move throughout the various device layers. **Figure 1(d)** illustrates the absorption spectra of all the various device layers from 300 nm to 800 nm. When evaluating the absorption spectra for the perovskite absorber, it is apparent that it strongly absorbs light across the visible range, typically between approximately 400 nm and 500 nm. The transport layers ITO, SnO2, and Spiro-OMeTAD appear to absorb very little light at wavelengths greater than approximately 400 nm which minimizes unwanted optical losses and thereby provides for more photons to be available for absorption in the perovskite absorber. The way light is arranged for maximum capture and charge extraction allows for both efficiencies to be achieved. With this arrangement the simulated device has a PCE of 24.57% under ideal optical conditions. Once the optical filter/ interface effects are included it drops to approximately 22.09% efficiency or a decrease of ~2.5% points.

International Journal of Engineering Research & Technology (IJERT)
ISSN: 2278-0181
Vol. 15 Issue 05 , May - 2026

Table 1: The table shows the physical parameters of the materials of the SC.

Parameters	Unit	ITO	SnO_2	$(BDA)(MA)_3Pb_4I_{13}$	Spiro-OMeTAD
Thickness	μm	0.02	0.06	0.9	0.06
Bandgap (E_g)	eV	3.5[9]	2.9[5]	1.62[10]	3.17[11]
Electron Affinity (χ)	eV	4.0	~3.9[12]	3.87	2.05
Dielectric permittivity (ε) (relative)	-	9.0	9.0	25.0	3.0
CB Effective density of states (N_C)	$1/cm^3$	$2.2x10^{18}$	$2.2x10^{18}$	$2.2x10^{18}$	$1x10^{20}$
VB Effective density of states (N_V)	$1/cm^3$	$1.8x10^{18}$	$1.8x10^{19}$	$1.0x10^{19}$	$1x10^{20}$
Electron thermal velocity (V_e)	cm/s	$1x10^7$	$1x10^7$	$1x10^7$	$1x10^7$
Hole thermal velocity (V_h)	cm/s	$1x10^7$	$1x10^7$	$1x10^7$	$1x10^7$
Electron mobility (μ_e)	cm^2/Vs	20	100	2.61	2.0
Hole Mobility (μ_h)	cm^2/Vs	10	0.256	5.0	0.01
Shallow uniform donor density (N_D)	$1/cm^3$	$1x10^{18}$	$1x10^{17}$	$1x10^{15}$	0
Shallow uniform acceptor density (N_A)	$1/cm^3$	0	0	$1x10^{15}$	$1x10^{19}$
Total defect density (N_t)	$1/cm^3$	$1x10^{15}$	$1x10^{15}$	$1x10^{14}$	$1x10^{13}$

III. RESULTS AND DISCUSSIONS

A. Optimization of Absorber Thickness

The perovskite layer will have optimum efficiency when the thickness is approximately (0.8-1.0) m, providing optimum light absorption and carrier movement without excessive losses. The fill factor is approximately (83%) at this range. The open-circuit voltage (V_{OC}) decreases with increasing thickness for thinner films such as those (~0.5 μm) yielding greater V_{OC} (~ 1.28 V) because there is less volume to recombine charges. On the other hand, thicker absorbers (~1.6 μm) will yield lower V_{OC} values (~1.22 V) because there are more defects along the carrier collection pathway. The short-circuit current density (J_{SC}) will also increase with increasing thickness because a thicker absorber can absorb more near-infrared photons. Below (0.5 μm), PCE values are between (23.8%) due to poor light absorption. The maximum PCE occurs between (0.8-1.0 μm) with a PCE of (24.57%) at which point the current collected equals the voltage retained. When the thickness is greater than (0.9 μm) the PCE drops to (24.2%) at (1.6 μm) because the charge carrier diffusion length is comparable to the thickness of the absorber, leading to recombination prior to reaching the device interfaces. There is a trade-off between the absorption of photons and recombination of charges. Under conditions where realistic optical filtering occurs, the device achieves (22.09%) PCE at its optimal thickness (0.9 μm), which represents a decrease of 2.5%. **Figure 2(a-b)** indicates the PCE and Fill Factor and the J-V characteristics indicate that the J_{SC} increases monotonically as the thickness is increased [13].

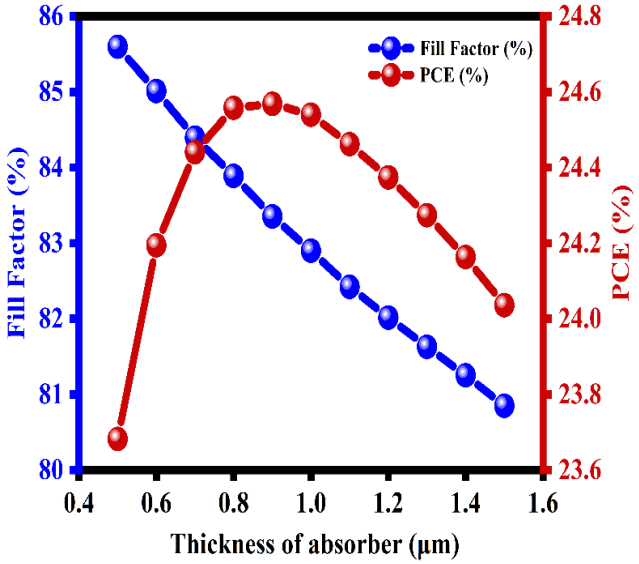

(a)

International Journal of Engineering Research & Technology (IJERT)
ISSN: 2278-0181
Vol. 15 Issue 05 , May - 2026

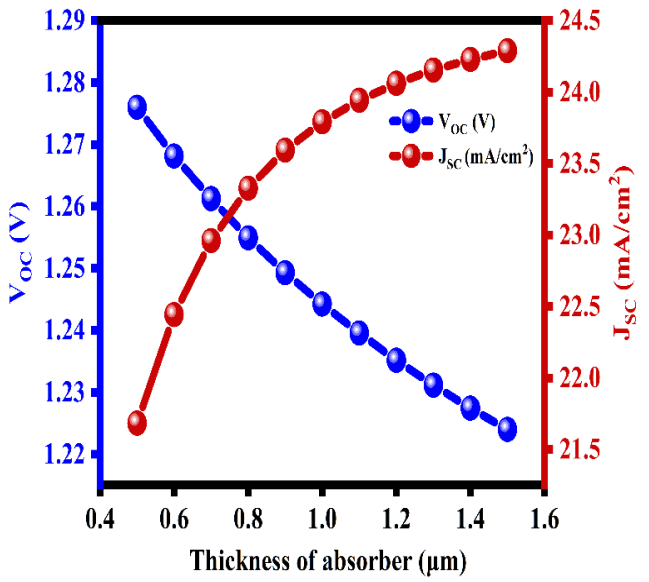

(b)

Fig. 2. Influence of Absorber Thickness on Performance Parameters: (a) PCE and fill factor; (b) Short-circuit current density and open-circuit voltage

B. Effect of defect density in the absorber on the solar cell

Photovoltaic devices have a defective device including both bulk and interface defects. The density of the defect is altered from 1×10^{10} cm^{-3} to 1×10^{20} cm^{-3} to examine the effects of these variations on the output parameters that were presented in **figure 3**. There is a reduction in the PCE of the device as defect densities are increased given in the figure. At low defect densities (10^{10}-10^{13} cm^{-3}) the PCE (~28-29%) and FF (~85-88%) are maintained almost constant because recombination is controlled by intrinsic radiative processes with the majority of photogenerated carriers being collected. As the defect density is increased above ~10^{14} cm^{-3}, deep trap states are created that promote Shockley–Read–Hall (SRH) recombination causing the carrier to have short life times. This significantly lowers V_{OC}, degrades diode ideality, and results in FF collapse upon increasing to 10^{18}-10^{20} cm^{-3}. The presence of both high levels of bulk recombination and creating potential shunting paths negatively impact upon PCE. Increased defect density (10^{18} cm^{-3}) provides less charge extraction and results in a collapse of J_{SC}. A defect density of ~10^{14} cm^{-3} will yield a high level of V_{OC}. Defect passivation via 2D interface will prevent recombination allowing parameters to be maintained. Defects in the absorber layer generate states that cause SRH recombination limiting solar cell performance. The SRH recombination is can be described with the following equation:[14]

$$R^{SRH} = \sigma_{n,p} V_{th} N_t \left(\frac{n_p - n_i^2}{n+p+2n_i \cos\left(\frac{E_t - E_i}{KT}\right)} \right) \quad (4)$$

where σ_n and σ_p represent the capture cross sections for electrons and holes, respectively, V_{th} is the thermal velocity of the particles, N_t is the total density of defects, E_t is the energy level of trapping defects, and E_i is the energy level of an intrinsic semiconductor.

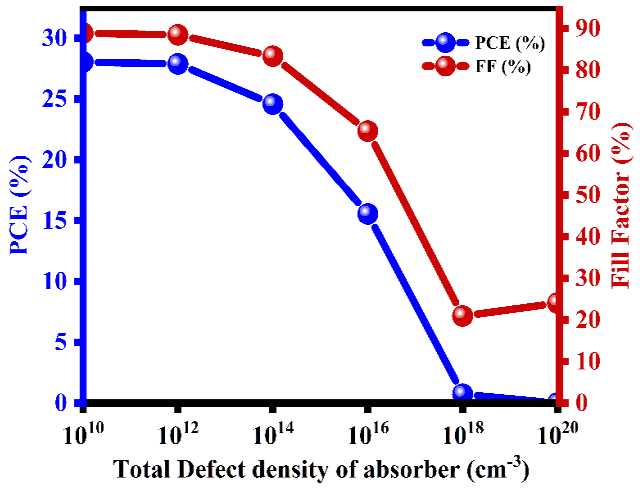

(a)

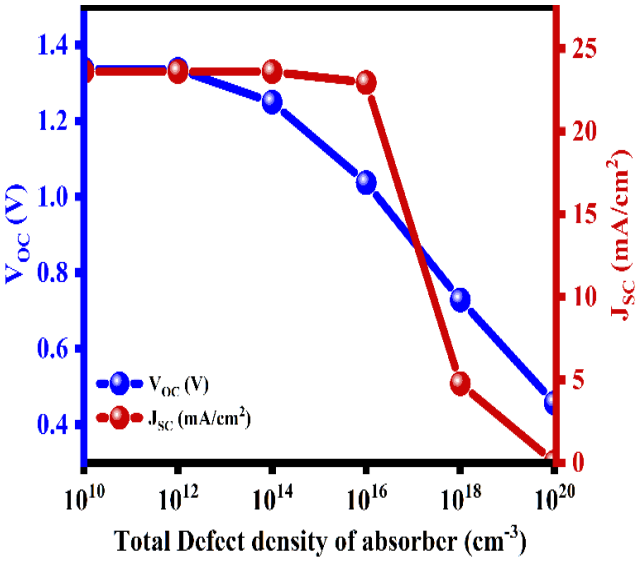

(b)

Fig. 3. Effect of absorber defect density: (a) PCE and fill factor; (b) Short-circuit current density and open-circuit voltage

C. Impact of temperature on solar cell PV parameters

From **Fig. 4**, the increase in temperature (280-350K) leads to a linear decrease in PCE and FF. This suggests that the increase in series resistance is dominating over recombination at elevated temperatures. As temperatures rise, the average energy of the electrons increases and the effective bandgap decreases, which causes V_{OC} to decrease, as shown in **Fig. 4.** The decrease in V_{OC} with temperature also follows the relationship given by Equation 5. [13]

$$V_{OC} = \eta V_T \ln\left(\frac{i_p + I_o}{I_o}\right) \quad (5)$$

With increasing temperature, reverse saturation current (I_o) also increases resulting in a decrease of Voc. V_T is thermal voltage and i_p is photo generated current.

Increasing temperature increases the amount of phonon scattering within the transport layers resulting in an increasing contact resistance. As a result, the Fill factor (FF) losses

International Journal of Engineering Research & Technology (IJERT)
ISSN: 2278-0181
Vol. 15 Issue 05 , May - 2026

correlate with the decline in power conversion efficiency (PCE) (approximately 25.4% to 22.4%). The two-dimensional (2D) layer will improve thermal stability by reducing ionic migration and keeping good interface quality via quantum confinement effects. V_{OC} decreases (approximately 1.28 to 1.17 V) because of the inverse relationship between temperature and the voltage produced by the photovoltaic device, while J_{SC} remains constant (approximately 23.600 mA/cm^2) due to the bandgap of the material shifting to shorter wavelengths, thus resulting in a decrease in sub-bandgap absorption losses. Therefore, although voltage produced by a photovoltaic device is the limiting factor in the overall efficiency of these devices, J_{SC} remains stable from high to low-temperature operation periods, which demonstrates better long term performance stability for a previously launched module.

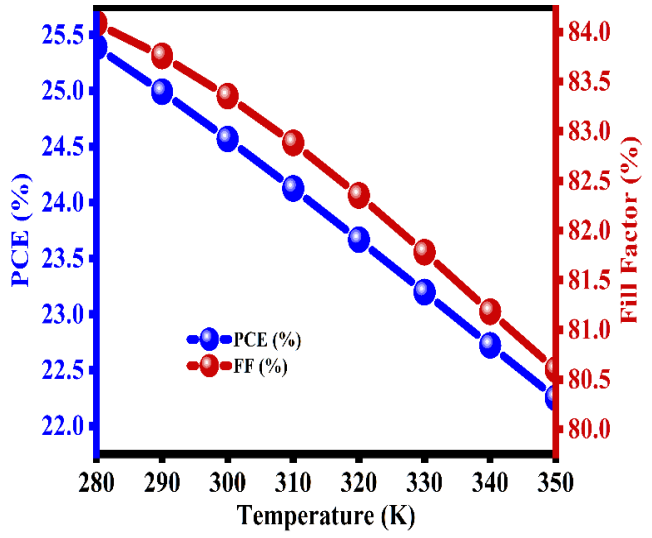

(a)

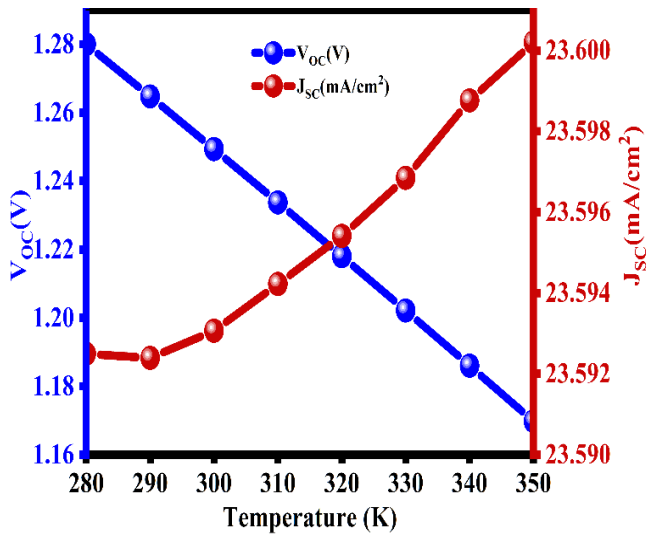

(b)

Fig. 4. Effect of temperature on performance parameters: (a) Power conversion efficiency (PCE) and fill factor (FF); (b) Short-circuit current density (J_{SC}) and open-circuit voltage (V_{OC})

D. J-V and EQE characteristics

The External Quantum Efficiency (EQE) of a solar cell is defined as the percentage of the incident photon's wavelengths that can produce carriers in a solar cell. EQE of $(BDA)(MA)_3Pb_4I_{13}$, with a bandgap of 1.62 eV, is approximately 90% (with optical filter) and is greater than 95% (without optical filter) (**Fig.5c-d**) over the range of 350–700 nm indicating good photon absorption over the entire visible spectrum. Below 300 nm, the EQE drops off due to the parasitic absorption of the transparent electrical contacts and transport electrical layers. The sharp cutoff at approximately 780 nm is due to the optical band edge where photons not have enough energy to excite electrons [15].

The J-V Curve offers information about the spatial layout of photogenerated carrier recombination, as well as the kinetic pathways that result in the recombination of photogenerated carriers. The external photocurrent is limited by the competition between the collection of photogenerated carriers and the non-radiative recombination of photogenerated carriers in forward-bias ($0 < V < 1.3$). In **Figures 5a-b**, J_{SC} can reach 21.256 mA/cm^2 when using an optical filter and 23.593 mA/cm^2 without using an optical filter[16].

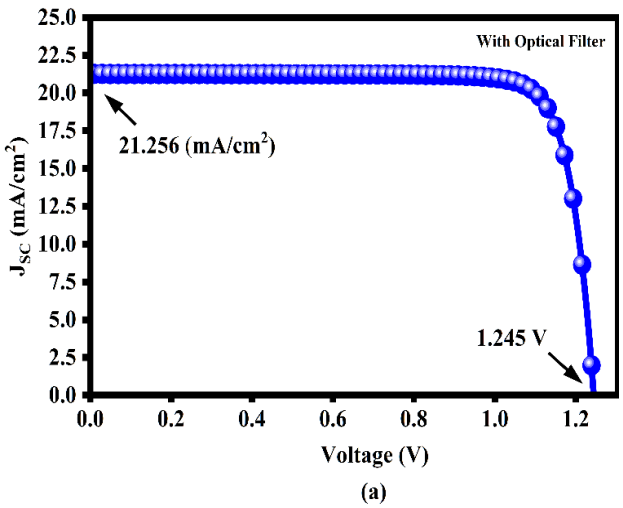

(a)

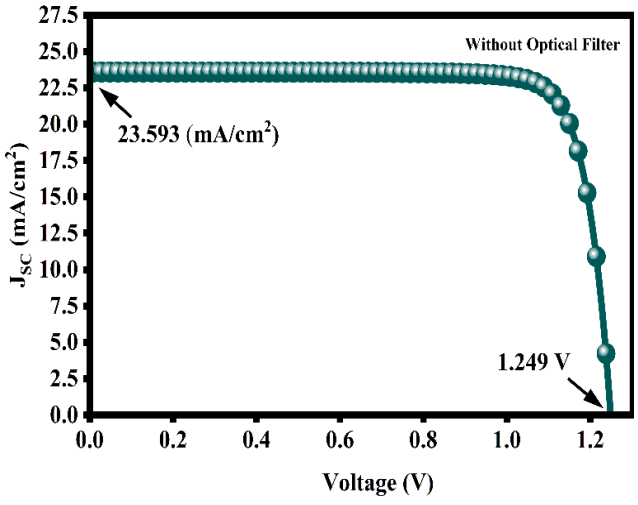

(b)

International Journal of Engineering Research & Technology (IJERT)
ISSN: 2278-0181
Vol. 15 Issue 05 , May - 2026

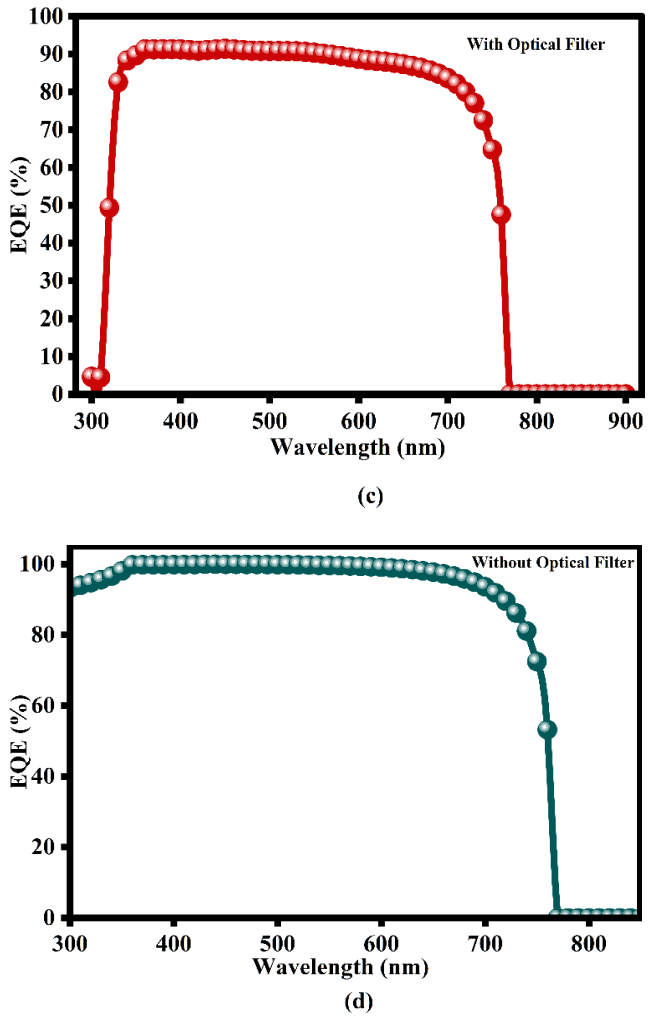

Fig. 5. Characteristics of proposed architecture: (a) J-V curve (with optical filter); (b) J-V curve (without optical filter); (c) EQE curve (with optical filter); (d) EQE curve (without optical filter)

E. Comparison of the Proposed Work with Various Simulated and Experimental Reported Works

Table 2 compares the optimized ITO/SnO_2/(BDA)$(MA)_3Pb_4I_{13}$/Spiro-OMeTAD/Au device with previously published experimental and theoretical results for both three-dimensional and two-dimensional (2D) perovskite solar cells. Because the theoretical (resulting from PCE) of the proposed 2D Dion-Jacobson device is 24.57% and the expected (based on real-world conditions for optical loss) is 22.09%, the performance metrics for the proposed architecture remain competitive with previously reported 3D perovskite devices. By optimizing the absorber layer thickness, defect density, and interface engineering simultaneously, the performance metrics of the proposed 2D solar cell architecture will be comparable with those published previously for 2D solar cells. Therefore, the SnO_2/(BDA)$(MA)_3Pb_4I_{13}$/Spiro-OMeTAD architecture will enable high-efficiency 2D photovoltaic devices exhibiting extended operational stability consistent with that of Dion-Jacobson-type materials.

Table 2: Comparison Between the Present Study and Previously Reported Results:

Parameter	Yang et al. (2018)[17]	Niu et al. (2019)[10]	Proposed Work
Anode	ITO	Not specified	ITO
ETL	EDTA-SnO_2	TiO_2/SnO_2	Pure SnO_2
Absorber	$MAPbI_3$ (3D)	BDA$(MA)_5Pb_5I_{16}$ (2D, n=5)	(BDA)$(MA)_3Pb_4I_{13}$ (2D, n=4)
HTL	Spiro-OMeTAD	Spiro-OMeTAD	Spiro-OMeTAD
Cathode	Au	Au	Au
PCE	20.64%	16.38%	24.57% (Ideal) / 22.09% (Realistic)
V_{OC}	~1.13 V	~1.04 V	1.2493 V (Ideal) / 1.2445 V (Realistic)
J_{SC}	~24 mA/cm^2	~20.01 mA/cm^2	23.59 mA/cm^2 (Ideal) / 21.26 mA/cm^2(Realistic)
FF	-	~78.64%	83.36% (Ideal) / 83.49% (Realistic)
Research Type	Experimental	Experimental	SCAPS-1D Simulation

International Journal of Engineering Research & Technology (IJERT)
ISSN: 2278-0181
Vol. 15 Issue 05 , May - 2026

IV. CONCLUSION

Through this paper, we explored the operation of ITO/SnO_2/(BDA)$(MA)_3Pb_4I_{13}$/Spiro-OMeTAD/Au solar cells using the SCAPS-1D simulation software. Specifically, we were focused on optimizing the design of the device and how different absorber thicknesses, defect concentrations, and temperatures will affect photovoltaic metrics. The optimization led to a theoretical maximum efficiency of 24.57% with V_{OC} = 1.2493 V; J_{SC} = 23.59 mA/cm^2 and FF = 83.36%. The use of optical filters caused the efficiency to drop to approximately 22.09%. These results highlight the necessity of achieving high-quality absorption materials and designing the device with proper geometry. To summarize, our optimized 2D Dion Jacobson configuration generates a highly-viable candidate for high-efficiency, thermally and environmentally stable perovskite solar cells, and will be good candidates for future experimental testing and device integration.

REFERENCES

[1] U. N. E. Programme and I. E. Agency, *2019 Global Status Report for Buildings and Construction: Towards a Zero-emissions, Efficient and Resilient Buildings and Construction Sector*, vol. 224. 2019. Accessed: Dec. 11, 2025. [Online]. Available:https://wedocs.unep.org/handle/20.500.11822/30950

[2] H. Tsai *et al.*, "High-efficiency two-dimensional ruddlesden-popper perovskite solar cells," *Nature*, vol. 536, no. 7616, pp. 312–317, Jul. 2016, doi: 10.1038/nature18306.

[3] G. E. Eperon, C. E. Beck, and H. J. Snaith, "Cation exchange for thin film lead iodide perovskite interconversion," *Mater Horiz*, vol. 3, no. 1, pp. 63–71, Dec. 2015, doi: 10.1039/C5MH00170F.

[4] L. Mao *et al.*, "Hybrid Dion-Jacobson 2D Lead Iodide Perovskites," *J Am Chem Soc*, vol. 140, no. 10, pp. 3775–3783, Mar. 2018, doi: 10.1021/jacs.8b00542.

[5] K. Monga, M. Aggarwal, V. Singh, and S. Chaudhary, "Zinc and [Zinc, Nickel]: Co-doped SnO2 nanoparticles as prospective electron transport layer materials for efficient lead free-MASnI3 perovskite solar cells," *Chemical Physics Impact*, vol. 8, Jun. 2024, doi: 10.1016/j.chphi.2024.100651.

[6] A. Slami and L. Merad, "Numerical Study of Based Perovskite Solar Cells by SCAPS-1D."

[7] M. Burgelman, K. Decock, A. Niemegeers, J. Verschraegen, and S. Degrave, "SCAPS manual."

[8] L. Lin *et al.*, "Boosting efficiency up to 25% for HTL-free carbon-based perovskite solar cells by gradient doping using SCAPS simulation," *Solar Energy*, vol. 215, pp. 328–334, Feb. 2021, doi: 10.1016/j.solener.2020.12.059.

[9] N. Rai, S. Rai, P. K. Singh, P. Lohia, and D. K. Dwivedi, "Analysis of various ETL materials for an efficient perovskite solar cell by numerical simulation," *Journal of Materials Science: Materials in Electronics*, vol. 31, no. 19, pp. 16269–16280, Oct. 2020, doi: 10.1007/s10854-020-04175-z.

[10] Y. Zheng *et al.*, "Oriented and Uniform Distribution of Dion–Jacobson Phase Perovskites Controlled by Quantum Well Barrier Thickness," *Solar RRL*, vol. 3, no. 9, Sep. 2019, doi: 10.1002/solr.201900090.

[11] A. Slami and L. Merad, "Numerical Study of Based Perovskite Solar Cells by SCAPS-1D."

[12] R. Mariappan, V. Ponnuswamy, P. Suresh, R. Suresh, M. Ragavendar, and C. Sankar, "Deposition and characterization of pure and Cd doped SnO2 thin films by the nebulizer spray pyrolysis (NSP) technique," *Mater Sci Semicond Process*, vol. 16, no. 3, pp. 825–832, Jun. 2013, doi: 10.1016/j.mssp.2013.01.006.

[13] A. K. Patel, R. Mishra, and S. K. Soni, "Performance Analysis of a Cu(In1−xGax)Se2 Solar Cell with Nontoxic WS2 and WSSe Buffer Layers," *J Electron Mater*, vol. 51, no. 11, pp. 6168–6179, Nov. 2022, doi: 10.1007/s11664-022-09863-6.

[14] A. Chetia, D. Saikia, and S. Sahu, "Design and optimization of the performance of CsPbI3 based vertical photodetector using SCAPS simulation," *Optik (Stuttg)*, vol. 269, no. July, p. 169804, 2022, doi: 10.1016/j.ijleo.2022.169804.

[15] S. Yadav, P. Lohia, and A. Sahu, "Enhanced performance of double perovskite solar cell using WO3 as an electron transport material," *Journal of Optics (India)*, vol. 52, no. 2, pp. 776–782, 2023, doi: 10.1007/s12596-022-01035-3.

[16] V. Srivastava, R. K. C. Pooja, and L. Shivangi, "Investigation of Eco - friendly Perovskite Solar Cell Employing Niobium Pentoxide as Electron Transport Material using SCAPS - 1D," no. 0123456789, 2024.

[17] J. W. Lee *et al.*, "2D perovskite stabilized phase-pure formamidinium perovskite solar cells," *Nat Commun*, vol. 9, no. 1, Dec. 2018, doi: 10.1038/s41467-018-05454-4.